Visualising chemical composition and reaction kinetics by the near infrared multispectral imaging technique

Chieu D. Tran

Department of Chemistry, Marquette University, Milwaukee, WI 53233, USA

A new multispectral imaging spectrometer which is capable of simultaneously recording spectral images in the visible and near infrared has been developed. In this instrument, an acousto-optic tunable filter (AOTF) is used to diffract an unpolarised incident light into two diffracted beams with orthogonal polarisation. One of the beams is detected by a silicon camera for the visible region while the other is detected in the near infrared (NIR) region (from 1000 to 1700 nm) with an NIR camera. The imaging spectrometer is sensitive, inexpensive and field deployable because it is based on a camera using the recently available InGaAs focal plane arrays which are low-cost and can be sensitively operated at room temperature. The imaging spectrometer was used for measurements which previously were not possible. These include the kinetic determination of curing of an epoxy resin by amine, and the detection of reaction products from solid-phase peptide synthesis. Rates of reactions between epoxy and amine were found to be very inhomogeneous. Because of this kinetic inhomogeneity, differences in the degrees of cure at different positions within the sample can be as high as 37% when data from only a single pixel were used for calculation. The inhomogeneity was not observed if the average of a large number of pixels was used. The NIR imaging spectrometer was also used for the kinetic determination and identification of products formed during the solid phase peptide synthesis of glycine, alanine and valine mediated by aminomethylstyrene resin beads. Because this NIR imaging spectrometer can measure spectra at different positions within a sample, it was used for the first demonstration in which reactions of three different solid-phase peptide syntheses (in a three-compartment cell) were simultaneously monitored. Since relatively good spectra can be obtained by using data recorded by a single pixel and because the NIR camera has 240×320 pixels, this NIR multispectral imaging technique is not limited to three-compartment cell used in this study but rather can be used as the detection method for solid-phase peptide synthesis in combinatorial chemistry.

Keywords: acousto-optic tunable filter, InGaAs focal plane arrays, imaging, combinatorial chemistry, epoxy resin, inhomogeneous, near infrared, modulation transfer function

A multispectral imaging spectrometer is an instrument which can simultaneously record spectral and spatial information of a sample, i.e. the recorded images contain signals that are generated by molecules or units in a sample, plotted as a function of spectral and spatial distribution.[1] Chemical distribution in a sample or chemical compositions of several samples can be elucidated from such images. The type information is of particular importance since it is known that chemical as well as physical properties of materials are dependent on the chemical distribution within the samples. As a consequence, considerable efforts have been made in the last few years to develop multispectral imaging instruments. In these instruments, a camera is used to record the spatial distribution of the sample, and the spectral information is gained by scanning a dispersive device to record spectra for each image.[1] Dispersive devices based on mechanical scanning (e.g.

filter wheels, monochromators) are not desirable because they are slow and prone to vibrations. Spectral tunable filters based on electronic tuning such as acousto-optic tunable filters, are desirable as they are fast, compact and have no moving parts.

An acousto-optic tunable filter (AOTF) is a solid state electronically tunable spectral bandpass filter which is based on the diffraction of light by an acoustic wave in an anisotropic crystal.[2–9] Compared to other dispersive devices, the AOTF offers such advantages as being all solid state, having rapid scanning ability (μs), high diffraction efficiency and wide spectral tuning range, giving high resolution (0.2–0.6 nm) and offering imaging capability.[2–9] Because of these advantages, the AOTF has been used to develop novel instruments which would not be possible otherwise. For example, novel spectroscopic instruments including the multi-dimensional fluorimeter,[3,4] the multi-wavelength thermal lens spectrometer,[9] fast-scanning UV/vis/NIR detectors for HPLC[5] and flow injection analysis[6] have been successfully developed using the AOTF. The AOTF is also suited for the development of a multispectral imaging instrument.

The objective of this work is to use the AOTF synergistically with an uncooled NIR camera based on InGaAs focal plane arrays which has become commercially available recently to develop a novel, inexpensive, highly-sensitive and field-deployable multispectral imaging instrument. Detailed information on the instrumentation development will be reported in this paper. Preliminary results on some of applications of the imaging spectrometer including the kinetic determination of curing of an epoxy resin by amine and the detection of peptides synthesised by solid-phase peptide synthesis will be described.

Instrumentation

Optical consideration

It is known that the AOTF has much wider spectral tuning range than conventional grating monochromators. Typically, it can be tuned from the visible to the NIR region. For example, the TeO_2 non-collinear AOTF which we previously used in our laboratory for the development of the detector for flow injection analysis (FIA) can be tuned from 600 to 1700 nm.[6] Additionally, because the AOTF crystal is anisotropic, an incoming unpolarised light will be diffracted by the AOTF into two beams (ordinary and extraordinary beam) with orthogonal polarisation. Because of these features, it is possible for a multispectral imaging instrument based on the AOTF to record images of a sample simultaneously in the visible as well as in the NIR regions. This can be accomplished by using an unpolarised light incident onto the AOTF to produce two diffracted beams; one of the diffracted beam will be used for the recording of images in the visible region (with a silicon CCD camera) and the other beam for the NIR images.

Camera consideration

Traditionally, a camera based on InSb focal plane arrays (FPA) is the most widely used camera for the infrared region. The main advantage of the InSb FPA camera is its reliability and wide spectral range (from 1000 to 5000 nm). While this wide tuning range is attractive, it is seldom that the whole range is utilised in multispectral imaging instruments. This is because the tuning range of instruments is usually governed not by the camera but rather by the dispersive device (e.g. AOTF). As a consequence, InSb FPA is widely used in the mid-IR region (from 3000 to 5000 nm) because it is the most sensitive detector in this region. Its use in the NIR region (from 1000 to 2500 nm) is not as widespread as in the mid-IR region because its sensitivity in this region is relatively lower than other NIR detectors. InGaAs detectors are known to have the highest sensitivity in the NIR region, and can operate at room temperature. The latter feature not only makes these detectors easier to use but also reduces the size and cost. As a consequence, InGaAs is usually the detector of choice for the NIR region. However, cameras based on InGaAs focal plane arrays were not available until recently. The 320×240 InGaAs FPA camera recently available from Sensors Unlimited Corporation makes it possible, for the first time, to develop a sensitive multispectral imaging instrument for the NIR region at a fraction of cost compared to those based on the InSb camera. The attractive features of this InGaAs camera including its low cost and high sensitivity. Specifically, its room temperature detectivity is 10^{13} Jones, giving it a great advantage over InSb, HgCdTe or PtSi sensors that require cooling. It is sensitive in the 900 to 1700 nm NIR region and its quantum efficiency is better than 70% from below 1000 to beyond 1600 nm.

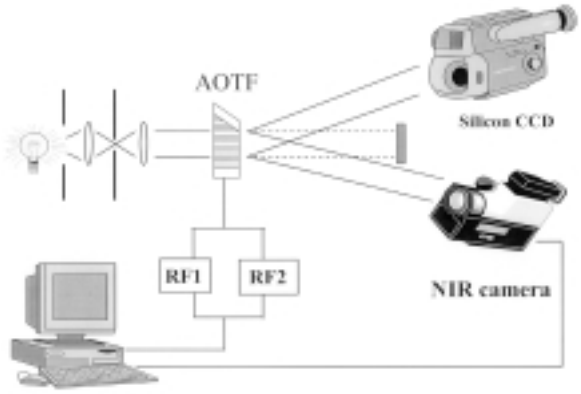

Figure 1. Schematic diagram of the imaging spectrometer: AOTF, acousto-optic tunable filter; RF, RF signal generator, CCD, charge-coupled device camera for the visible; FPA, InGaAs focal plane array camera for the NIR region.

Multispectral imaging spectrometer

Figure 1 shows the schematic diagram of the multispectral imaging instrument. As illustrated, light from a 250 W halogen tungsten lamp was collimated by a lens prior to passing through a non-collinear TeO_2 acousto-optic tunable filter (Matsushita Electronic Components Co., Ltd, Model EFL F20R2). Two RF generators were used to drive the AOTF; one with a frequency range of 96 to 53 MHz for the visible region (650 to 1050 nm) and the second for the NIR region (1000 to 1650 nm) with a frequency range of 59 to 35 MHz. The signals from these generators were amplified by a RF power amplifier (Minicircuits Model MAV-11) before being connected to the AOTF. In addition to the transmitted beam, the AOTF diffracted unpolarised incident light into two diffracted beams that have orthogonal (horizontal and vertical) polarisation. As illuminated, two diffracted beams not only have orthogonal polarisation but also are spatially separated. One of the diffracted beams was used to record spectral imaging in the visible region while the other was for the NIR region. It is important to point out that because the AOTF crystal is anisotropic and the two diffracted beams have orthogonal polarisation, the two beams will have a slightly different wavelength when an RF signal is applied to the AOTF. It is, therefore, important to calibrate the relationship between the applied RF frequency and the wavelength of the diffracted beam separately for each beam. The spectral images in the visible region were recorded by a thermo-electrically cooled silicon charge coupled device (CCD) UV/visible camera (Spectral Source Instruments, Model HPC-1) which has 512×512 pixels and is sensitive in the UV and visible region (from 200 to 1100 nm). This silicon CCD camera does not detect any light at wavelength longer than 1100 nm. Initially, a NIR camera based on InGaAs focal plane arrays (FPA) (Sensors Unlimited Model SU18-1.7RT/RS170), equipped with 128×128 pixels and which was sensitive in the 1000 to 1700 nm, region was used to record images in the NIR (from 1000 to 1650 nm). Subsequently, an InGaAs camera with higher resolution (320×240 pixels) was used for kinetic measurements of an epoxy resin and as a detector for combinatorial chemistry. The sensitivity of the InGaAs cameras in the visible is negligible, i.e. no light at wavelength shorter than 1000 nm is detected by the cameras. Images in the visible were differentiated from those in the NIR by sequentially scanning the RF drivers and recording the images with the corresponding visible or NIR camera. Alternatively, the two RF drivers were synchronised with the corresponding cameras to facilitate the simultaneous recording of the visible and the NIR region. A digital frame grabber was used to transfer images from the cameras to a microcomputer for imaging processing.

Performance characteristics of the imaging spectrometer

A modulation transfer function (MTF) was used to evaluate the resolution of the imaging spectrometer. Definition of the MTF can be found elsewhere.[10,11] The MTF values of the instrument in the visible region at 650 nm, and in the NIR region at 1400 nm were determined by use of the USAF 1951 resolution target. For comparison, the MTFs for the system in which the AOTF was replaced by interference filters at 650 and 1400 nm were also determined. The results obtained are shown in Figure 2 (a and b). The MTFs obtained with the filters are similar to those obtained with the AOTF at the corresponding wavelengths. This suggests that any image perturbations induced by the AOTF are too insignificant to be observed in the system. The image quality in the visible is much better than that in the NIR. This can be explained by the differences in resolution of the two cameras, namely the CCD camera used to record visible images has a much better resolu-

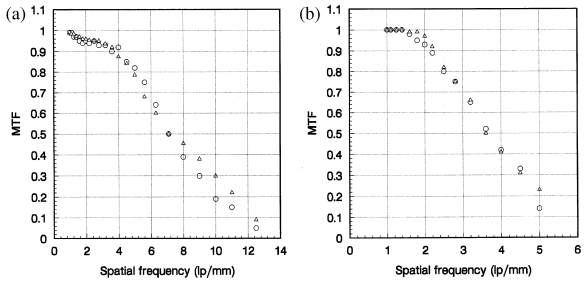

Figure 2. Plot of Modulation Transfer Function (MTF) as a function of spatial frequency or line pair per mm ($lp\,mm^{-1}$) measured at: (a) 650 nm with the CCD camera and at 1400 nm (b) with the InGaAs camera: (O) with AOTF and (Δ) with interference filter.

tion than the NIR camera. Specifically, the visible CCD camera is equipped with an SI-502A sensor (Scientific Imaging Technology, Inc., Oregon, USA). This sensor has 512×512 pixels, and each pixel is 24 µm×24 µm. This corresponds to 20 pairs mm^{-1} in the horizontal as well as in the vertical direction. Conversely, the pixel size of the FPA NIR camera is 60 µm×60 µm and there are 128×128 pixels in this camera. This corresponds to only about 8 pairs mm^{-1}, and that may be the main reason for the lower imaging quality in the NIR. Better resolution was obtained when the 10-bit 128×128 InGaAs camera was replaced by the 12-bit camera which has 320×240 pixels with 40 µm×40 µm pixel size.

Applications

Kinetics of curing of epoxy by amine

The NIR technique has been used extensively in recent years for the chemical analysis of individual polymers, the chemical compositions of copolymers, and the kinetic of polymeric reactions.[12–17] For example, it was demonstrated recently that the kinetics of the cure reaction of an epoxy resin by amine can be determined by NIR.[12–17] While such applications clearly demonstrate the potential and utilisation of the NIR method it is important to realise that care must be taken in such measurements to avoid possible errors. The concerns are due to the nature of the polymers and NIR instruments used for their measurements. Specifically, polymeric samples are known to be chemically inhomogeneous, and because of the chemical inhomogeneity, rates of a polymer reaction may be different at different positions in a sample. As a consequence, the polymeric end-product may not be chemically homogeneous. Since chemical and physical properties of polymers depend on their chemical compositions, the presence of chemical inhomogeneity will have pronounced effects on their properties. It is, therefore, important that the rate of a polymeric reaction can be measured at different positions in a polymer sample in order to determine the presence of any kinetic inhomogeneity. Unfortunately, to date, NIR-based kinetic methods rely on the use of NIR spectrometers equipped with single channel NIR detectors.[12–16] As such, it has not been possible to determine kinetics of a reaction simultaneously at different positions in a polymer sample. The present NIR multispectral imaging spectrometer is particularly suited for such requirements.

Curing of the epoxy [poly(bisphenol-A-co-epichlorohydrin) glycidyl end capped] resin by amine (diethylenetriamine) was investigated using the NIR multispectral imaging instruments. The reaction between the epoxy resin and the amine is given in Scheme 1. The epoxy–amine cure reaction was initiated by vigorously mixing the two compounds for five minutes with a glass rod in a beaker in stoichiometric proportion, namely the concentration of epoxy was twice the concentration of amine. This ratio is known to produce a 3D-network during the cure reaction.[12,16,18] The mixture was then introduced to a home-made cell which consists of an aluminium frame with two glass windows separated by a 3 mm-thick rubber frame spacer. The cell was placed in a home-made cell holder equipped with a thermal coupler, a heater and a temperature controller for the recording, controlling and maintaining the temperature of the cell.

Images of the mixture of epoxy and amine at 25°C were recorded for each wavelength from 1000 to 1700 nm at 5 nm intervals (by scanning the AOTF). From these images, NIR absorption spectra of the epoxy–amine mixture at different times can be determined.

Kinetic determination

Shown in Figure 3 are the NIR spectra of the sample at different reaction times (from 0 to 8 h). The band, which is initially centred at 1527 nm, can be attributed to the first overtones of the primary and secondary

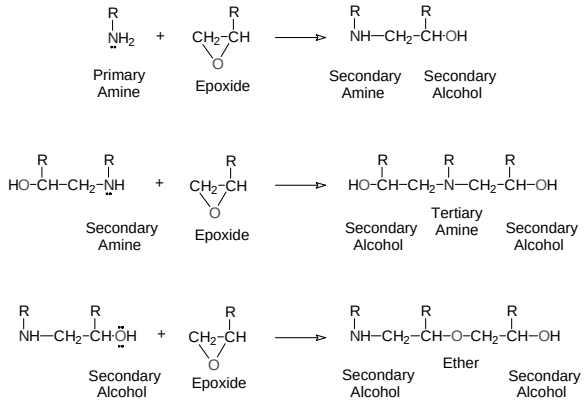

Scheme 1. Curing of epoxy resin by amine.

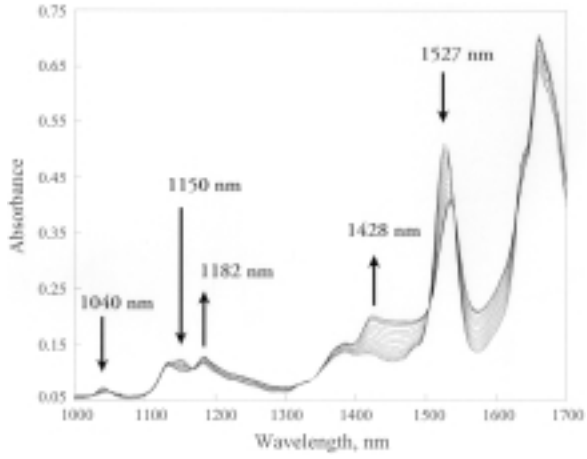

Figure 3. NIR absorption spectra of epoxy–amine mixture during an eight-hour cure at room temperature (25°C), shown at an interval of 15 min. Spectra were calculated from averaged absorbance of a square of 30×30 pixels of images recorded with the NIR multispectral image instrument.

amine groups. The band at 1428 nm can be assigned to the first overtone of the hydroxy functionality. Between 1100 and 1200 nm there are three bands. These bands can be attributed to second overtones of different C–H groups, namely the aromatic C–H at 1132 nm, the epoxy C–H at 1150 nm and the aliphatic C–H at 1182 nm. The kinetics of the epoxy–amine cure reaction can be monitored by use of one or all of three absorption bands: the epoxy band at 1150 nm, the hydroxy band at 1428 nm and the amine band at 1543 nm. The hydroxy band at 1428 nm was selected for the kinetic measurements. The selection was made because this band has relatively large changes, fewer errors and no interference from other bands. The degree of cure reached at the end of the reaction was determined from the NIR spectrum of the cured epoxy measured with a NIR spectrophotometer equipped with a single channel InGaAs detector. The measurements were performed at the epoxy band at 2201 nm at the beginning (t=0) and the end of the cure (t=225 minutes). It was found that 50% of cure was obtained at 25°C. This value is comparable to the value of 65% obtained for the reaction between bisphenol-A epichlorohydrin resin and 1,6-hexanediamine at 30°C.[12]

As illustrated in Scheme 1, in the initial step, epoxy reacts uncatalytically with amine to produce hydroxy-amine compound. As the hydroxy-amine compound is formed, its hydroxy group catalyses the subsequent reaction between amine and epoxy. This type of reaction is known as autocatalysed reaction. The hydroxy groups also can react with epoxy to form an ether to stop the reaction. Consequently, the overall reactions can be considered as uncatalysed initiation, autocatalysis and inhibition. Based on this model, the relationship between the degree of cure, α, and rates of reactions can be expressed as.[12,14,20–22]

$$\frac{d\alpha}{dt} = (k_a + k_b\alpha^n)(\alpha_\infty - \alpha)^m \qquad (1)$$

In addition to the degree of cure α, an additional term α_∞ is used because the maximum cure in this case was 90% (at 55°C). This empirical expression can be explained as follows: the reaction at the beginning is uncatalysed and has a rate constant of k_a. Subsequently, the reaction proceeds via autocatalysis by the hydroxy group with a rate constant of k_b. Because the O–H group is formed during the curing reaction, this term is multiplied by the degree of cure α^n (i.e. $k_b\alpha^n$). Finally, the reaction becomes slower when α approaches α_∞ (inhibition).

Curve fitting of experimental data to Equation 1 was performed to obtain values for k_a, k_b, α_∞. They were found to be 6.8×10^{-4}, 3.6×10^{-2} and 0.50, respectively. It seems that the k_b value (3.6×10^{-2}) is several times larger than the k_a value (6.8×10^{-4}). This is hardly surprising considering the fact that k_a is representative of an uncatalysed reaction whereas k_b is characteristic of a reaction catalysed by O–H groups. The values of m and n were found to be 0.91 and 1.63, respectively, which are comparable with values of 0.85 and 1.39 reported for a similar epoxy–amine system.[12]

Figure 4. Images of epoxy–amine during a cure at 50°C, recorded at 1428 nm and at different times: $t=0$ (a), $t=7$ min (b) and $t=50$ min (c).

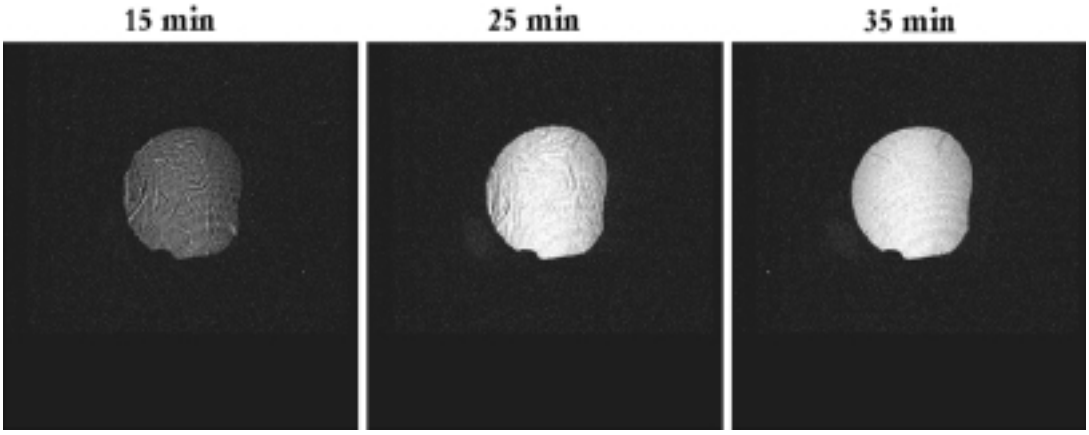

Figure 5. Differential images of the epoxy–amine, obtained by subtracting the image recorded at 1390 nm (background) from that at 1428 nm at different times: 15, 25 and 35 min.

Kinetic inhomogeneity

The spatial inhomogeneity of an epoxy–amine cure was subsequently investigated. Figure 4 shows the NIR images at 1428 nm of the epoxy–amine mixture at 50°C at time $t=0$, 7 and 50 min. Spatial inhomogeneity was clearly observed at 0 and 7 min. This is probably due to a non-uniform mixing of the epoxy resin and the amine. This inhomogeneity disappeared when the mixture reached the preset temperature of 50°C which took about 10 min from the start of the reaction. The temperature fluctuation at the beginning is due to the experimental procedure. Specifically, in this experiment, the cell holder was preheated at 50°C. When the cell reached that temperature, the heater was removed for about 2 min in order to insert the sample into the cell holder. It took about 10 min for the temperature of the sample to reach a constant temperature of 50°C (the two components, epoxy and amine can not be preheated at 50°C because the reaction occurs very fast at this temperature so that the two chemicals start to react during the mixing).

As described previously, the kinetics can be determined by monitoring the hydroxy band at 1428 nm. Any differences in the reaction rate within the epoxy–amine sample can be readily observed by subtracting the image recorded at 1390 nm (background signal, no band) from the image recorded at 1428 nm (hydroxy band). The resulting pictures are shown in Figure 5 for epoxy–amine mixture at 50°C recorded at 15, 25 and 35 min after the reaction started. As described in previous section, most of the cure occurs in this time interval. It is evidently clear from the pictures that the cure reaction at any given time is not homogenous, especially during the accelerated phase of the reaction (*c.* 15–25 min). When most of the cure is completed, the kinetic inhomogeneity becomes less pronounced.

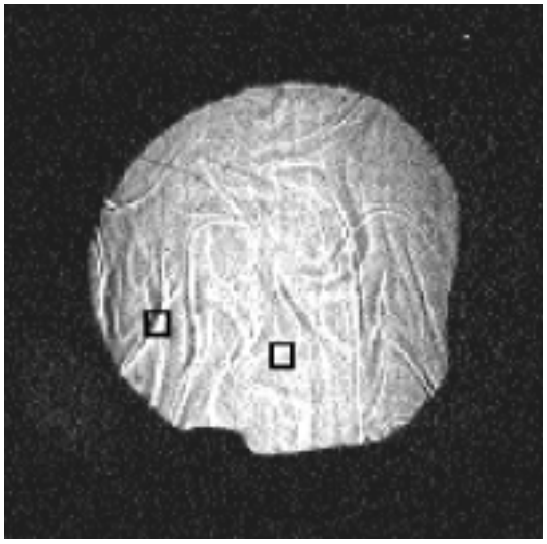

Figure 6. Enlarged image of epoxy-amine at 50°C, recorded at 1428nm and at 15minutes after the reaction started. The two squares represent areas from which data from a single pixel were selected.

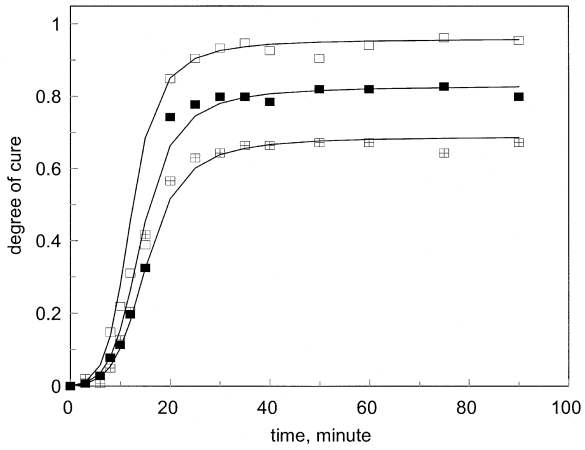

Figure 7. Plot of degrees of cure as a function of time for epoxy–amine mixture at three different positions in the sample: single pixel corresponds to the bright spot shown in Figure 6 (□), the dark spot (⊞) and to an average of 60×60 square pixels (■).

Evidence for kinetic inhomogeneity can be clearly observed in the following example. Shown in Figure 6 is the image of the epoxy–amine at 50°C, recorded at 1428nm, and at 15min after the reaction started. It illustrates the presence of inhomogeneity in the sample, which is due mainly to the differences in reaction rates at different positions in the sample. The inhomogeneity can be quantitatively presented by fitting data collected at three different positions: data from an averaged intensity of a 60×60pixel square; data from a "bright" single pixel (as illustrated in Figure 6) and data from a "dark" single pixel (as illustrated in Figure 6). Best fits of experimental data, shown in Figure 7, indicate that up to 96% cure was obtained at the bright single pixel spot, 84% for the average of 60×60pixels and only 70% for the dark single pixel spot. These results clearly demonstrated that because of the kinetic inhomogeneity, up to 37% difference in the degrees of cure can be observed at different positions within the sample.

The inhomogeneity can only be observed when kinetics are simultaneously determined at different positions in the sample with a camera having high spatial resolution. In other words, the observed inhomogeneity is dependent on the spatial resolution of the imaging spectrometer. No inhomogeneity will be observed if signals from all pixels of the camera are averaged. This conclusion is based on the results in Table 1 which lists the degrees of cure for the dark and bright spots when different numbers of pixels were used for each spot to fit Equation 1. When only one pixel was used per each spot to fit, the degrees of cure were found to be 96% and 70% for the bright and dark spot, respectively. The α_∞ value for the bright spot decreases to 84% whereas that for the dark spot increases to 73% when a square of 3×3pixels were used per each spot for fitting. In fact, as the number of pixels per each spot increases, the degree of cure for the bright spot decreases and that for the dark spot increases so that they approach the value of 84% which was obtained when a square of 60×60pixels were used for fitting. Of course, no inhomogeneity will be observed if a single channel photodiode (such as those used in conventional NIR spectrometers) is used as detector.

Conclusions

In summary, it has been demonstrated that the high sensitivity and fast scanning ability of the newly-developed NIR multispectral imaging spectrometer make it suitable for kinetic determination of fast reac-

Table 1. Degrees of cure calculated for the bright and dark spot shown in Figure 6 with different numbers of pixels per spot.

	Degree of cure, %	
Number of pixels	Bright spot	Dark spot
1	96	70
3×3	88	73
5×5	88	77
7×7	86	77
9×9	86	79
20×20	85	80
30×30	84	82
40×40	84	83
50×50	84	84
60×60	84	84

tions. As expected, when used to determine the kinetics of the curing of an epoxy resin by an amine, the data obtained by this imaging instrument agree well with those obtained by FT-IR. The imaging spectrometer thus, possesses all advantages of conventional NIR spectrometers. It has, however, additional features which conventional IR spectrometers cannot offer, namely, its ability to provide kinetic information at different positions within a sample. The high spatial resolution and sensitivity of the InGaAs camera make it possible to determine the kinetics from data collected by a single pixel in the camera. The kinetics of curing of an epoxy resin by an amine, determined by this multispectral imaging instrument show that the reaction rates within the sample are very inhomogeneous, and because of this inhomogeneity the differences in the degrees of cure reached at different positions within the sample can be as high as 37%. The cross-link density of the epoxy is, therefore, inhomogenous. This will have a pronounced effect on a variety of materials including advanced fibre reinforced composites (AFRC) as it is known that epoxy and amine hardener systems are widely used in AFRCs, and that the mechanical properties of AFRCs are dependent on the cross-link density of the epoxy.

Detector for combinatorial chemistry

The use of combinatorial synthesis in drug discovery has increased significantly in the last few years.[23–26] Vast numbers of compounds can be quickly and readily prepared by combinatorial synthesis using solid-phase synthesis on polymer substrates.[23–25] Innovative analytical methods which are capable of non-destructive and *in situ* monitoring and analysis of such immense numbers of compounds are, therefore, needed. Conventional analytical techniques such as TLC, HPLC, GC and MS are not suitable since they require cleavage of the compound of interest from the polymeric support.[23–25] Magic angle spinning NMR technique can be used to analyse (solvent) swollen resin. However, it suffers from low sensitivity and long acquisition time, and hence is not suited for the analysis of high sample throughput and reaction kinetics.[23–25] Near and mid-infrared imaging methods are probably the most promising techniques.[26–33] Infrared techniques have been successfully used to monitor and to analyse products of solid-phase combinatorial reactions.[26–33] However, the application of the IR technique in combinatorial chemistry is still limited because of the relatively slow speed, and high cost associated with the FT-IR instruments. An FT-IR instrument equipped with a microscope was required in almost all of these studies.[26–33] In addition to the high cost, such an instrument can measure only a single position in a sample. When measurements are made on a large number of compounds as in combinatorial synthesis, it is slow, labour intensive and also prone to errors. An infrared method which is capable of rapidly and simultaneously acquiring spectral information of a large number of samples is, therefore, desirable. Multispectral imaging spectrometer can offer a solution for this problem. A mid-infrared multispectral imaging spectrometer has been recently developed. This instrument is based on the use of the conventional FT-IR for spectral scanning and a HgCdTe focal plane array camera as the detector.[34–36] This instrument has been successfully used to determine properties of polymers.[37] However, its use as the detector for combinatorial chemistry has not been explored. The complexity and high cost associated with this instrument may be one of the factors that limit this type of application. The AOTF-based NIR multispectral imaging spectrometer developed in our laboratory is particularly suited for such application because of it simplicity, inexpensive and robustness.

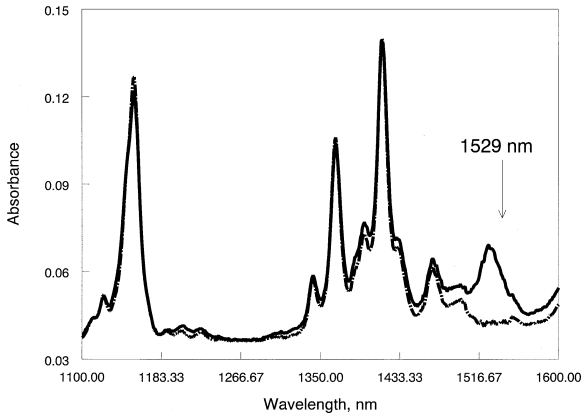

Figure 8. Absorption spectra of the aminomethylstyrene beads in methylene chloride (solid line), and methylene chloride alone (dotted line).

Experimental procedure

Aminomethylstyrene resin beads (Polymer Laboratories, Amherst, MA, USA) which have a loading of 1.9 mmol g^{-1} and size of 400–500 µm were used in this study for the solid-phase peptide syntheses. The resin beads were dispersed in methylene chloride and allowed to equilibrate for at least one hour so that the beads can swell to a constant size. The NIR spectra of methylene chloride alone, and of the swollen beads in CH_2Cl_2 (in a 2 mm pathlength cell) were measured using the multispectral imaging instrument (Figure 8). As illustrated, the only difference between two spectra is the single well-resolved band at 1529nm. This band is due to the first overtone of the N–H stretching vibration of the amino groups attached to the beads. Since these immobilised amino groups are involved in all solid-phase syntheses, this result indicates that it is possible to use the NIR multispectral imaging technique to monitor the solid-phase reaction based on these beads.

Initially, a single compartment cell was used. This cell was constructed from aluminium with two microscope slides as windows to provide a clear optical aperture of 4×2 cm, and a pathlength of 7.5 mm. The cell has an inlet at the top and an outlet at the bottom. Porous glass frits were installed at its outlet to keep the beads inside and to allow the solvent to flow freely at a high flow rate through the cell. Three different amino acids, namely glycine, alanine and valine, were used in this study. The amino groups of these amino acids were protected with the *N*-fluorenylmethoxycarbonyl (Fmoc) protecting group. The peptide synthesis was carried out in three steps: activation of the amino acid, coupling reaction and deprotection of the amino group.

To activate an amino acid three equivalents (relative to the amount of amino groups on the solid support) of the amino acid was initially dissolved in a minimum amount of DMF (about 2 mL). Subsequently, four equivalents of 1,3-diisopropyl-carbodiimide (DIC) in 1 mL of chloroform was then added, and the mixture was allowed to equilibrate for 2 min to activate the carboxylic acid group completely.

The activated amino acid was then added to the reactor cell which contained 250 mg of resin suspended in a minimum amount of chloroform. The NIR images of the mixture were recorded by the NIR multispectral imaging instrument after this addition, and the recording continued for at least two hours to monitor the coupling reaction. Upon completion, the beads were washed five times with chloroform and the final spectrum of the beads was recorded in pure chloroform.

The removal of the Fmoc protecting group was accomplished by washing the beads three times (for five minutes each) with 20% piperidine in DMF, and then five times with chloroform. The NIR spectra were then recorded. The resin support was now ready to be linked with a second amino acid.

The absorption spectra were calculated by using the average intensity over 60×60 pixels in each picture (a total set of 161 pictures were recorded from 1440 to 1600 nm). Each spectrum shown is an average over five recordings.

Solid-phase peptide synthesis in a single compartment cell

The spectra taken for each step of the synthesis of an Ala-Ala-Ala tripeptide are shown in Figure 9. The starting resin *(beads-NH_2)*, shown as Spectrum (a), has a band at 1529 nm. This band is similar to that obtained for the same beads recorded in the previous calibration step (Figure 8). A new band at 1483 nm is observed in Spectrum (b) which is for the product obtained after the first coupling reaction *(beads-NH-Ala-Fmoc*). This band can be attributed to the two amide groups in the coupling product. This coupling reaction is estimated to be close to 100% because the absorption of the amino group on the beads at 1529 nm for this *(beads-NH-Ala-Fmoc)* is nearly zero. Spectrum (c) was obtained

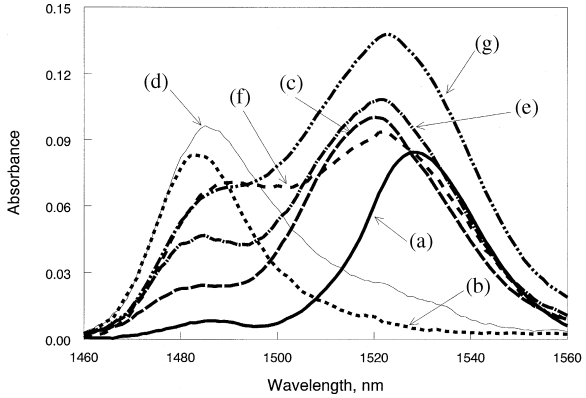

Figure 9. Absorption spectra during a tripeptide synthesis of alanine on aminomethylstyrene beads: (a) beads-NH_2, (b) beads-NH-Ala-Fmoc, (c) beads-Ala, (d) beads-Ala-Ala-Fmoc, (e) beads-Ala-Ala, (f) beads-Ala-Ala-Ala-Fmoc and (g) beads-Ala-Ala-Ala.

after removing the Fmoc protecting group (*beads-NH-Ala*). As illustrated, in addition to the amide band at 1483nm, this spectrum also has another band at about 1529nm. This is as expected because this band is due to the amino group generated in the compound after removing the Fmoc protecting group. The spectrum of the product of the second coupling reaction (*beads-NH-Ala-Ala-Fmoc*) is shown in Spectrum (d). This spectrum has a large amide band at 1483nm. However, there is also a small shoulder at about 1529nm. Since this shoulder is in the same wavelength region as that of the amino group observed in Spectrum (a), it is possible that the second coupling reaction was not completed even after two hours. Removing the Fmoc protecting group of this compound enabled the recording of Spectrum (e) for (*beads-NH-Ala-Ala*). This spectrum has two bands: 1483 and 1529nm. The first band is due to the amide bond. The intensity of this band is about two times higher than that of the Spectrum (c) [for *(beads-NH-Ala*)]. This is as expected because there are two amide bonds in (*beads-NH-Ala-Ala*) but only one in (*beads-NH-Ala*). The amino band at 1529nm for this dipeptide [(Spectrum (e)] has, as expected, similar intensity as that of the single coupling compound [Spectrum (c)]. Spectrum (f) is for the product obtained after the third coupling (*beads-NH-Ala-Ala-Ala-Fmoc*). Because the amine band at 1529nm is still present in the spectrum, it seems that the third coupling reaction could not be brought to completion. This is probably due to a lack of reacting time and/or mixing. The spectrum for the (*beads-NH-Ala-Ala-Ala*), obtained after removing the Fmoc protecting group is shown in Spectrum (g). As illustrated, the amine band at 1529nm is still of high intensity in this spectrum.

Solid-phase peptide synthesis in a multi-compartment cell

A new multi-compartment cell was constructed to demonstrate that the NIR imaging technique can be used to monitor not only a single reaction but rather many different reactions simultaneously. This cell has three different compartments. A rubber frame made from Viton was placed between the aluminium frame and the two-microscope glass slide windows to prevent the flowing of the sample from one compartment to the others. Each compartment has a clear optical aperture of 2×40mm. Similar to the single compartment cell, this multi-compartment cell also has an inlet and outlet for each of its compartments, and glass frits were installed at the outlet to keep the beads inside the cell and to allow the solvent to flow through. The cell pathlength was reduced from 7.5 to 5mm.

The NIR spectra of the beads in each of the three compartments are shown as the solid, dotted and dot-and-point lines in Figure 10(a). These spectra were calculated from the same set of NIR images, but at different positions corresponding to each compartment of the cell. As expected, the spectra of the beads are the same in all three compartments of the cell.

Alanine, glycine and valine were used as reactants for each compartment. The spectra obtained after the first coupling for each compartment are shown in Figure 10(b). It is evident that coupling reactions were successful because a pronounced amide band at 1483nm was observed in all three spectra [Figure 10(b)]. The spectra for glycine (solid line) and alanine (dashed line) are very similar to the spectra obtained after the first coupling in a single compartment cell [Spectrum (b) in Figure 9]. These results seem to indicate that the coupling reactions were completed for alanine and glycine. In the case of valine, the unreacted amine band at 1529nm is relatively higher, and the amide band at 1483nm is lower than those for alanine and glycine. This seems to imply that the coupling efficiency for valine is much lower than those for alanine and glycine. As expected, removing the Fmoc protect-

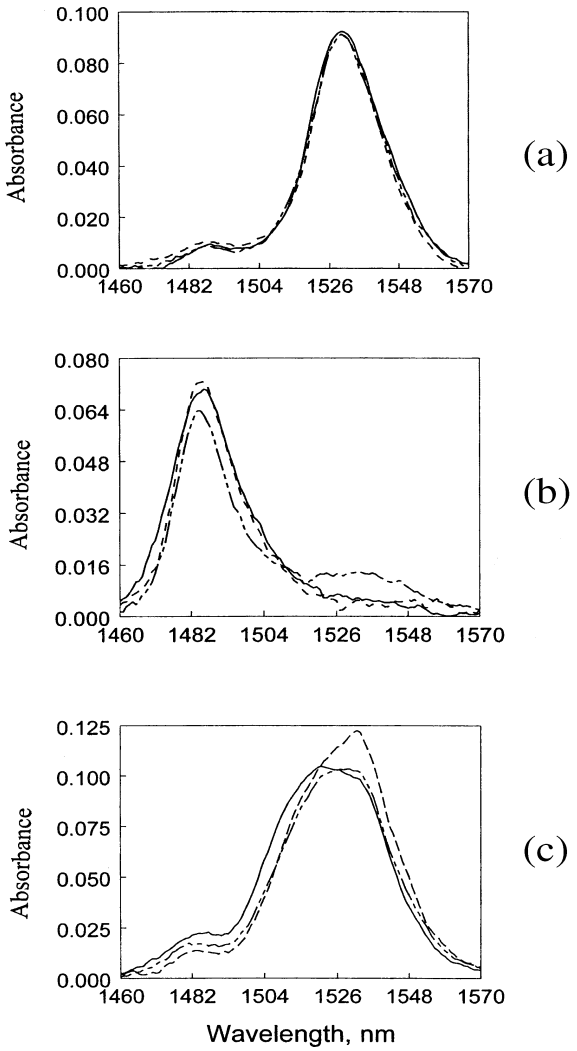

Figure 10. (a) Absorption spectra of the aminomethylstyrene beads in each compartment of the three-compartment cell; (b) Absorption spectra of the coupling products between the beads and valine (— ·· — ··), glycine (———) and alanine (– – –); and (c) Absorption spectra of the coupling products after removing the Fmoc protecting groups for valine (— ·· — ··), glycine (———) and alanine (– – –).

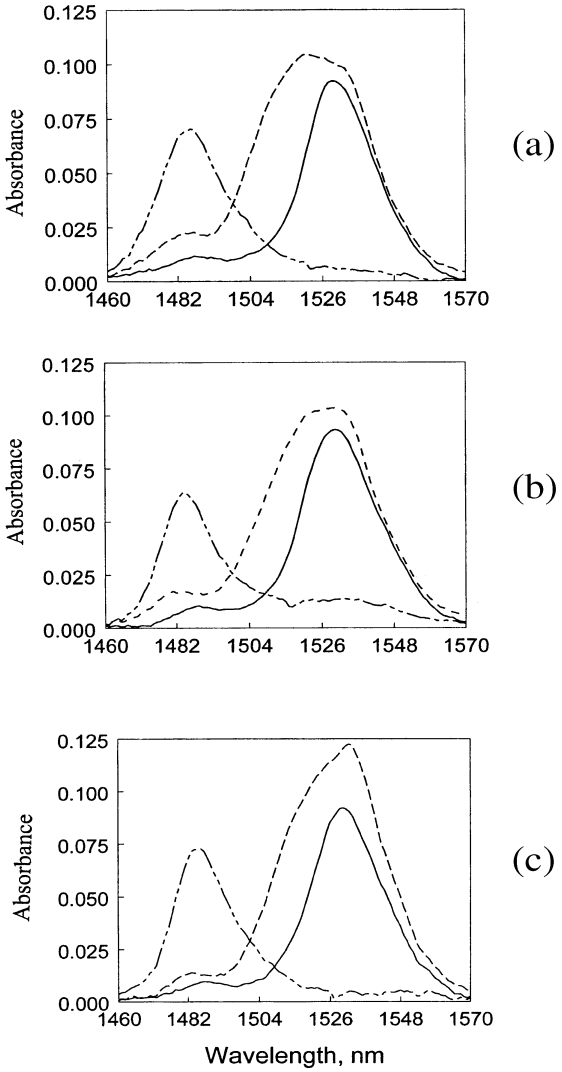

Figure 11. Changes in the absorption spectra of the starting resin beads, the FMOC coupling product and the detected coupling product measured in a three-compartment cell for glycine (a), valine (b) and alanine (c). (_____) are the spectra of the starting resin (———), (— ·· — ··) are the spectra of the coupling products and (----------) are the spectra of the products after removing the Fmoc protecting groups.

ing groups of the coupling products leads to the regeneration of the amine band at 1529nm [Figure 10(c)].

The spectra of each step of the reaction were plotted for each individual amino acid. The spectra of the beads before the reaction (*Beads-NH_2*), after the coupling (*Beads-NH-Amino acid-Fmoc*) and after removing the Fmoc protecting group (*Beads-NH-Amino acid*) for glycine are plotted in Figure 11(a). Similarly, those for valine and alanine were plotted in Figure 11 (b and c), respectively. As illustrated, glycine, valine and alanine were successfully coupled to the amine groups on the beads. The amine band at 1529nm for

the final product is higher than that in the starting resin for all three amino acids. This is rather unexpected because after removing the Fmoc protecting group, the number of NH_2 groups on the final product should be the same as that on the starting beads. The higher absorbance at 1529 nm observed in the final deprotected products may be due to the differences in the absorption coefficients of the amino groups on the beads and those on the amino acid final products. This difference was also observed for the experiments in the single compartment cell [in Figure 9, the absorbance at 1529 nm is higher for Spectrum (a) than for Spectrum (c)].

Conclusions

Taken together, it is evident that the solid-phase peptide synthesis can be successfully monitored by using the newly-developed NIR multispectral imaging spectrometer. This NIR imaging instrument possesses all the advantages of conventional NIR spectrometers, i.e. it can be used for the non-invasive monitoring of the reactions and identification of the products during the solid-phase peptide syntheses of glycine, alanine and valine mediated by aminomethylstyrene resin beads. The reaction was determined by monitoring either the decrease of the band at 1529 nm, which is due to the amino group on the beads or the increase of the amide band at 1483 nm. The amine band at 1529 nm was also used to determine the presence of the Fmoc protecting groups, and the efficiency of their removal. Additionally, this NIR imaging spectrometer has extra features which conventional NIR spectrometers cannot offer, namely, its ability to measure spectra at different positions within a sample. This feature was utilised for the first demonstration in which reactions of three different solid-phase peptide syntheses (in a three-compartment cell) were simultaneously monitored. As expected, the kinetics obtained for three reactions are similar to those obtained when each of the reactions was individually determined. It is important to realise that the number of compartments of the cell used for this study is not limited to three. Multi-compartment cells including those used in combinatorial chemistry (e.g. cell with 96×96 compartments) can be used. Furthermore, in this study, up to 16×16 pixels were used to calculate a spectrum for each sample. However, as demonstrated in the previous section, a relatively good spectrum can be obtained by using data recorded by a single pixel. Since the NIR camera used in this camera is equipped with 240×320 pixels, it is evident that this NIR multispectral imaging technique can be effectively used as the detection method for the solid-phase peptide synthesis in combinatorial chemistry. That is, this NIR imaging spectrometer should be able to monitor solid-phase peptide syntheses simultaneously in a multi-compartment cell equipped with 96×96 compartments or more. This possibility is the subject of our intense study.

Acknowledgement

The author is grateful Yan Cui, Marc Fischer, Xu Liu and Sergey Smirnov for their assistance. Acknowledgement is made to the National Institutes of Health, National Center for Research Resources, Biomedical Technology Program for financial support of this work.

References

1. M.D. Morris, *Microscopic and Spectroscopic Imaging of the Chemical State*. Marcel Dekker, New York (1993).
2. C.D. Tran, *Anal. Chem.* **64,** 971A (1992).
3. C.D. Tran and M. Bartelt, *Rev. Sci. Instrum.* **63,** 2939 (1992).
4. C.D. Tran and R.J. Furlan, *Anal. Chem.* **64,** 2775 (1992).
5. C.D. Tran and R.J. Furlan, *Anal. Chem.* **65,** 1675 (1993).
6. C.D. Tran and J. Lu, *Anal. Chim. Acta* **314,** 57 (1995).
7. M.S. Baptista, C.D. Tran and G.H. Gao, *Anal. Chem.* **68,** 971 (1996).
8. M.S. Baptista and C.D. Tran, *Appl. Opt.* **36,** 7059 (1997).
9. C.D. Tran and V. Simian, *Anal. Chem.* **64,** 1419 (1992).
10. M. Bass, *Handbook of Optics*. McGraw-Hill, New York, Vol. 2, Ch. 32, pp 32.1–32.10 (1995).
11. C.S. Williams and O.A. Becklund, *Introduction to the Optical Transfer Function*. John Wiley, New York (1989).
12. P.A. Crosby, G.R. Powell, G.F. Fernando, C.M. France, R.C. Spooncer and D.N. Waters, *Smart.*

Mater. Struct. **8,** 415 (1996).
13. Z. Shen and J.R. Schlup, *J. Appl. Polym. Sci.* **67,** 267 (1998).
14. J.H. Fu and J.R. Schlup, *J. Appl. Polym. Sci.* **49,** 219 (1993).
15. J. Xu and J.R. Schlup, *J. Appl. Polym. Sci.* **67,** 895 (1998).
16. N. Shimoyama, S. Hayano, K. Matsukawa, H. Inoue, T. Ninomiya and Y. Ozaki, *J. Polym. Sci. B* **36,** 1529 (1998).
17. A. Khettry and M.G. Hansen, *Polym. Eng. Sci.* **36,** 1232 (1996).
18. G.A. George, P. Cole-Clarke, N.S. John and G. Friend, *J. Appl. Polym. Sci.* **42,** 643 (1991).
19. D.W. Schiering, J.E. Katon, L.T. Drzal amd V.B. Gupta, *J. Appl. Polym. Sci.* **34,** 2367 (1987).
20. B.G. Min, Z.H. Stachurski and J.H. Hodgkin, *Polymer* **34,** 4483 (1993).
21. K.C. Cole, J.J. Hechler and D. Noel, *Macromolecules* **24,** 3098 (1991).
22. R. Ruff and I.G. Csizmadia, *Organic Reactions: Equilibria, Kinetics and Mechanism*. Elsevier, Amsterdam (1994).
23. A. Czarnik, *Anal. Chem.* **70,** 378A (1998).
24. A. Czarnik and A.W. DeWitt, *A Practical Guide to Combinatorial Chemistry.* American Chemical Society, Washhington, DC (1996).
25. S.R. Wilson and A. Czarnik, *Combinatorial Chemistry, Synthesis and Application*. John Wiley, New York (1997).
26. K. Russell, D.C. Cole, F.M. McLaren and D.E. Pivonka, *J. Am. Chem. Soc.* **118,** 7941 (1996).
27. D.E. Pivonka, K. Russell and T. Gero, *Appl. Spectrosc.* **50,** 1471 (1996).
28. D.E. Pivonka and T.R. Simpson, *Anal. Chem.* **69,** 3851 (1997).
29. B. Yan, G. Kumaravel, H. Anjaria, A. Wu, R.C. Petter, C.F. Jewell and J.R. Wareing, *J. Org. Chem.* **60,** 5736 (1995).
30. B. Yan and Q. Sun, *J. Org. Chem.* **63,** 55 (1998).
31. T.Y. Chan, R. Chen, M.J. Sofia, B.C. Smith and D. Glennon, *Tetrahedron Lett.* **38,** 2821 (1997).
32. H.U. Gremlich and S.L. Berets, *Appl. Spectrosc.* **50,** 532 (1996).
33. W. Li and B. Yan, *Tetrahedron Lett.* **38,** 6485 (1997).
34. P. Colarusso, L.H. Kidder, I.W. Levin, J.C. Fraser, J.F. Arens and E.N. Lewis, *Appl. Spectrosc.* **52,** 106A (1998).
35. C.M. Snively and J.L. Koenig, *Appl. Spectrosc.* **53,** 170 (1999).
36. C. Marcott, R.C. Reeder and D.L. Wetzel, *Vibrational Spectrosc.* **19,** 123 (1999).
37. C.M. Snively and J.L. Koenig, *Macromolecules* **31,** 3753 (1998).

Received: 8 November 1999
Revised: 2 February 2000
Accepted: 8 February 2000